
Check for updates

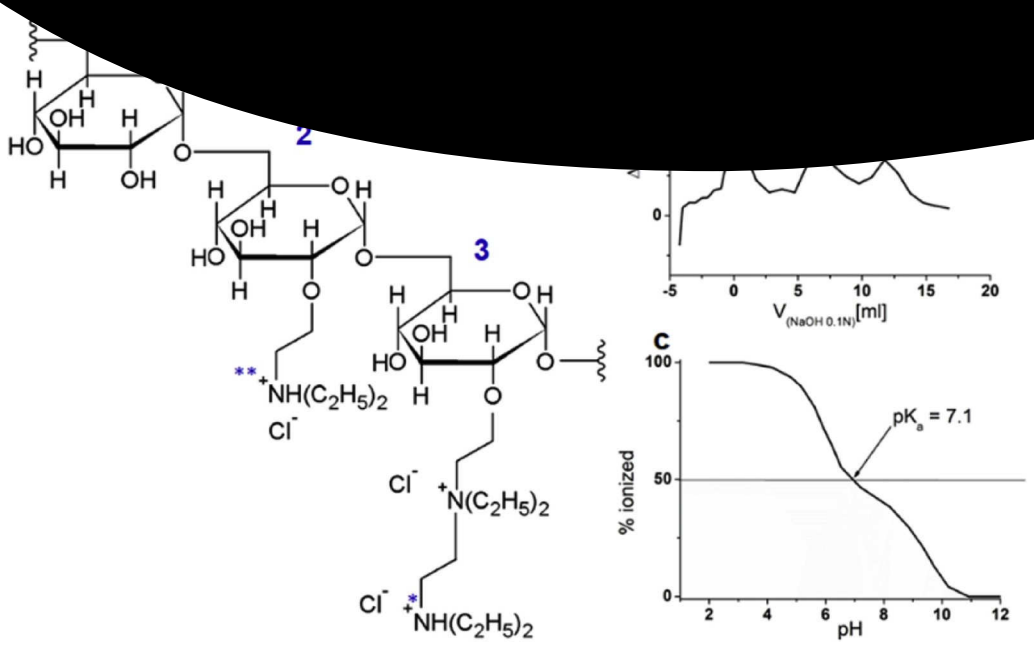

...mers of 6:1:1. Mole... weight is approx. 40 kDa. A total of 200 monomers is estimated. **b)** ΔpH/ΔV of 1.0 g DEAE-Dextran. * shows the peak position of the weaker tertiary amine,** of the stronger tertiary amine. **c)** Ionization of the tertiary amines of DEAE-Dextran. The pKa of the two tertiary amines is 7.1. The amount of nitrogen is 2.72% in dry mass.

Dextran may also be used as a coating of liposomes [19,20].

Small-angle x-ray (SAXS) and neutron (SANS) scattering are powerful characterization methods for investigation of colloidal systems, biomembranes, polymers, as well as RNA – [21–23]. SANS is a powerful complementary method to SAXS, where scattering occurs through interaction of neutrons with the nuclei instead of X-rays with the electrons, which therefore enables to generate scattering profiles with complementary contrast conditions. In particular, due to the differences between the scattering lengths between deuterium and hydrogen, it allows an insight into the distribution of water and the structure of materials by deuterium contrast variation (D-contrast). Although SANS measurements require more complex instrumentation (neutron sources), as well as more time and material, the possibility of contrast variation in SANS measurements offers the opportunity to match the scattering length density of a selected component, such that these becomes transparent to neutrons and the other moieties are highlighted [24–27]. Such advanced characterization may provide valuable basic information for development of pharmaceutical products by providing in-depth process understanding, process control, and guidelines for defining the range of acceptable process and product parameters (specifications) for the drug product [28].

In this work, SANS and SAXS measurements were applied to improve understanding of the molecular organization inside pharmaceutical polyplex nanoparticles, as formed from DEAE-Dextran and mRNA in different molecular ratios. The DEAE-Dextran to mRNA ratio was expressed as the charge ratio (N/P ratio) between the positive charges in the DEAE-Dextran and the negative charges in the mRNA. Previously it has been shown, that the charge ratio between cationic lipids and mRNA in lipoplex nanoparticles allows accurate control of the *in vivo* targeting selectivity after intravenous injection, enabling to develop a new class of i.v. injectable RNA immunotherapeutics against cancer up to the level of clinical studies [5,6]. For lipid-based mRNA formulations it has been shown that concise characterization with different complementary methods enables to reveal the organization in detail and to derive structure-function coherencies [29]. Here we have applied for the first time the principle of charge ratio variation for assembly of polymer based delivery vehicles comprising DEAE-Dextran as a model system, and used advanced methods such as SAXS/SANS for characterization of the molecular organization inside these systems.

2. Materials and methods

2.1. Materials

DEAE-Dextran (lot: 101114, MW 40 kDa, stretched length approx. 50 nm) was provided by Pharmacosmos (Holbaek, Denmark). mRNA with approximately ~2000 bases was synthesized by internal protocols at BioNTech RNA Pharmaceuticals GmbH (Mainz, Germany) (lot: 12-56-20, MW 681 kDa, stretched length approx. 560 nm, coiled length approx. 30–70 nm) [30–33]. Anhydrous D(+)-Glucose (lot: K46419537525) was purchased from Merck KGaA (Darmstadt, Germany). BioScience-Grade HEPES (lot: 294215827), hydrochloric acid (HCl), sodium hydroxide (NaOH) and nuclease free water was purchased from Carl Roth GmbH &Co. KG (Karlsruhe, Germany). For release of mRNA, European pharmacopeia reference standard Heparin (lot: Y0001282 Batch 2.1) was purchased from Sigma-Aldrich (St. Louis, MO, USA). Size measurements were performed with Y195.1 cuvettes and ζ potential measurements with DTS1070 cuvettes from Malvern Instruments Ltd. (Worcesterhire, United Kingdom). For RiboGreen®-Assay the Quant-iT kit (lot: 1709963) was used from Thermo analytics Inc. (Novi, MI, USA) and measured in 96-well plates. All other materials used were of analytical grade. RNAseZap was purchased from Ambion-Life Technologies (Carlbad, CA, USA). SANS specimens were investigated in Quartz cuvettes of 1 and 2 mm path length from Hellma. The D_2O samples were prepared from 99.75% D_2O from Merck KGaA (Darmstadt, Germany).

2.2. Methods

2.2.1. Potentiometric titration and N/P ratio calculation

For characterization of DEAE-Dextran, 1.0 g DEAE-Dextran was solubilized in 50 ml bidistilled water. As titrant, 0.1 N HCl and 0.1 N NaOH was used. Briefly, titrant was added stepwise through a volumetric burette and the change in electrical potential was measured using a WTW pH-meter pH538 (Xylem Inc., NY, USA) and a WTW SenTix 61 electrode. Titration of HCl was performed first to obtain a titration starting point for NaOH-titration. Titration was performed in triplicates for both NaOH and HCl. ΔpH/ΔV was plotted against the volume of the titrant (Fig. 1b). The exact amount of nitrogen was calculated by the volume of titrant, the molarity of titrant, and the molar mass of nitrogen (eq. (1)). The amount of the weaker tertiary amine is

eq
The am
(eq. (2)) and p

$$C_{nitrogen}[\%] = \frac{V_{titrant}[ml] * c_{titrant}[}{m_{DEAE-Dextran}[mg]}$$

$$ionized[\%] = \frac{V_{(NaOH)}[ml] + V_{(NaOH\ when\ 100\%of\ tertiary\ amine\ is\ ionized)}[ml]}{V_{(NaOH\ when\ 0\%of\ tertiary\ amine\ is\ ionized)}[ml]} \quad (2)$$

AG, H
was measured as described above.
was added stepwise as titrant until the ζ potential changed from positive to negative. The measured amount of free DEAE-Dextran was subtracted from the given amount to gain the actual amount of polymer in the particle.

2.3. Preparation of polyelectrolyte particles

For preparation of polyplexes, DEAE-Dextran and mRNA stock solutions were prepared. DEAE-Dextran was dissolved in 5% (w/w) glucose solution buffered with 10 mM HEPES at pH 7.2 and stirred for 1 h at room temperature. Briefly, volumetric equivalents of the polymer stock solution were added to the diluted mRNA stock solution at different N/P ratios, i.e. the ratio between mRNA phosphorus and DEAE-Dextran nitrogen, and gently vortexed for 10 s. Afterwards, particles were stirred for 1 h at room temperature. For SAXS measurements, 0.31 mg/ml (N/P ratio 2) and 1.55 mg/ml (N/P ratio 10) DEAE-Dextran were added to 0.1 mg/ml mRNA. For SANS measurements 1.24 mg/ml (N/P ratio 8) was added to 0.1 mg/ml mRNA. The discrepancy between the N/P ratios measured at either SAXS or SANS was due to technical requirements for measurement. However, the physicochemical characteristics are not supposed to change. The final buffer of all measured nanoparticles in SANS contained 2% glucose, 10 mM HEPES and 0.9% (0.154 M) NaCl. The buffer is thereby a slightly simplified version of HBSS, which is a cell culture buffer. This buffer can directly be inserted in cell cultures and was used as biorelevant transport medium for nanodrugs before [34]. The sodium bicarbonate, present in blood and intestinal fluid, was omitted in order to gain pH stable samples. For SANS measurements of the polyplexes, particles were manufactured in H_2O-buffer and 77.8% D_2O buffer. Other D_2O concentrations were blends of these two solutions.

2.4. Particle size and ζ potential measurement

Average particle size, size distribution and ζ potential were determined by dynamic light scattering on a Malvern Nano ZS (Malvern Instruments Ltd., Worcesterhire, United Kingdom) with the Zetasizer Software 7.11 at laser wavelength of 633 nm. For size measurements, backscattering detection at an angle of 173° was used. Particle sizes, given as $Z_{average}$ in nm, and polydispersity, given as polydispersity index, PDI, were obtained by fitting the correlation function using the cumulant method. The samples were either diluted to 0.05–0.1 mg/ml in 5 mM NaCl solution or diluted to 0.5–1 mg/ml in 154 mM NaCl solution and measured at 25 °C. ζ potential was measured at a concentration of 0.01–0.02 mg/ml in 5 mM NaCl and 25 °C. Calculation was done automatically using the Smoluchowski approximation [35]. Each measurement was repeated with at least two independent samples and measured in triplicate. A design space was created by increasing DEAE-Dextran concentrations in terms of N/P ratio.

2.5. mRNA and DEAE-Dextran concentration determination

For evaluating the mRNA concentration, Quant-iT™ Ribogreen® RNA reagent and kit from Invitrogen was used. Experimental procedure was performed according to the manufacturers' guideline. Briefly, samples were diluted and centrifuged, fluorescent dye was added and the fluorescence intensity was detected. For analysis, a Tecan infinite F200 plate reader (Tecan Group Ltd., Männedorf, Switzerland) was used. The excitation wavelength was 465 nm and emission wavelength 535 nm. The measurement was performed from below and the gain was

2.6. Heparin release assay

Particles containing 0.1 mg/ml mRNA were mixed with Fetal bovine serum (FBS) at equal volumes, resulting in a final FBS concentration of 50%. The mixture was incubated at 37 °C for 20 min. Subsequently, 10 µl heparin solution (10 mg/ml in 500 mM NaCl) was added to 90 µl sample at an increasing anionic/cationic mole ratio (N/P ratio) at pH 7.2 and incubated again at 37 °C for 20 min. As a control, an equal volume of HBGx1 was used to replace heparin solution. The heparin concentration was varied to identify suitable concentrations for the release of the mRNA. The free mRNA was detected using gel electrophoresis. Gel contained 1% Agarose, gel red and TBE-Buffer. Electrophoresis running time was 45 min at 114 V with a MSChoice10 electrophoresis from Biozym Scientific GmbH (Hessisch Oldendorf, Germany). The images were taken with a Typhoon Trio + from GE Healthcare (Little Chalfont, UK) with 532 nm green laser and 610BP30 emission filter.

2.7. Transfection and cell viability

mRNA cell transfection includes the attachment to the cell, endocytosis into the cell, the endosomal release, as well as the protein expression inside the cell and thereby serves as general proof of activity. Luciferase coding mRNA was used to transfect cells with DEAE-Dextran polyplexes. Dendritic cells (DC) were extracted from human blood, washed and seeded in 40 µl OptiMEM in 96 well plates (5×10^3 cells/well). 10 µl of diluted formulation was added, shortly shaken at 300 rpm and centrifuged at 300 G for 4 min. Respectively, a luciferase assay (Bright-Glo Luciferase kit, Promega, Madison, WI, USA) was performed 6 h post-treatment. Additionally, the viability of transfected cells was evaluated by the XTT cell proliferation Kit II (Sigma Aldrich GmbH, St. Louis, MO, USA). Readout was done 4 h after incubation with XTT reagent according to specifications. All measurements were performed using a TECAN infinite P200 PRO (Tecan Group Ltd., Männedorf, Switzerland). The wavelengths were set to 450 and 630 nm. As positive control, untreated cells were used. Viability was calculated according to eq. (3):

$$Cell\ viability\ [\%] = \frac{treated\ cells - blank}{untreated\ cells - blank}\ x\ 100 \quad (3)$$

2.8. Small angle x-ray scattering/small angle neutron scattering

2.8.1. Measurement

The structure of DEAE-Dextran/mRNA polyplexes was investigated by x-ray (SAXS) and neutron (SANS) small-angle scattering measurements. SAXS measurements were conducted at the EMBL P12 BioSAXS beamline at PETRA III, DESY (German Electron Synchrotron Hamburg, Germany) at an x-ray energy of 10 keV and a flux of 5×10^{12} ph/s [36]. The beam size at the sample position was $0.2 \times 0.3\ mm^2$ (v x h, full width half maximum, FWHM). Samples were measured in standard batch mode measurements using the P12 robotic sample changer [37] continuously flowing the solution in an in-vacuum quartz capillary while collecting the SAXS data. 2D SAXS patterns of the samples were recorded by a PILATUS 2 M detector, azimuthally averaged and corrected for the respective background/solvent signal to obtain the 1D

pre
KWS2
MLZ, Garching
vector) calculated fro
wavelength $\lambda_x = 1.24$ Å and the
common q-range in SAXS measurements was 0.0
to-detector distance of 3 m and for SANS measurement 0.0015–0.5 $Å^{-1}$ at three sample-to-detector distances 2 m, 8 m and 20 m. The neutron beam size at the detector was 6 × 8 mm^2. Samples with low D_2O-content were measured in quartz cells with 1 mm path length and higher D_2O-concentrations (≥33%) with 2 mm path length. Background from the buffer, and the quartz cell, as well as the incoherent scattering was subtracted and normalized to the neutron flux monitored during irradiation time and transmission. After that, the data from three sample-to-detector distances were merged. Further data reduction steps, such as intensity scaling, and radial integration were performed with Origin 2016 (Origin Lab, Massachusetts, USA).

Scattering vector, momentum transfer

$$q = \frac{4\pi}{\lambda}\sin\theta \tag{4}$$

2.8.2. Analysis

Model-based analysis of the SAXS experimental data was done using the unified exponential power law from the multi-level *Beaucage* model (eq. (5)) [38,39] implemented in the *SASfit* 0.94.10 software package [40]. This model allows to describe large composite particle like structures made out of smaller sub-particles. Therein, each structural, i.e. composite particle and sub-particle, is described by two pre-factors (G_i, B_i) and two structural factors (R_i, P_i). G/G_s are the Guinier pre-factors of the larger/lower structural level, B/B_s are pre-factors specific to the type of power-law scattering. Here, R_{g1} is the radius of gyration of the low q-value structures, i.e. corresponding to the size of the larger particle. R_{sub}/R_s represent the radius of gyration for the smaller structure. P/P_s are the scaling exponents of the power law assigned to the specific structural levels. To reduce the amount of fitting parameters monodispersity was assumed for the model fitting. Nevertheless, polydisperse solutions are present, therefore only apparent radii of gyration are obtained by this analysis. First approximate values of P and P_s were obtained by measuring the decay of the scattering curves. The corresponding parameters determined by the fitting procedure are given in table S1 (supplementary data). In case of R_{g1} only approximate values can be given, as the length of the actual R_{g1} is beyond the resolution of the instruments.

Beaucage equation

$$I_{Beaucage}(Q) \cong G\exp\left(-\frac{Q^2R_{g1}^2}{3}\right) + B\exp\left(-\frac{Q^2R_{sub}^2}{3}\right)\left(\frac{\left[\operatorname{erf}\left(\frac{QkR_{g1}}{\sqrt{6}}\right)\right]^3}{Q}\right)^P + G_s\exp\left(-\frac{Q^2R_s^2}{3}\right) + B_s\left(\frac{\left[\operatorname{erf}\left(\frac{Qk_sR_s}{\sqrt{6}}\right)\right]^3}{Q}\right)^{P_s} \tag{5}$$

The pair-distribution function P(r) can be calculated through a Fourier transform of the scattering curve (eq. (6)). Indirect Fourier transform methods have been developed for calculating P(r) [41–43]. The intraparticular pair distance distribution was obtained using the program GNOM [42] of the ATSAS software package [44]. The pair distance distribution functions were calculated with the following boundary conditions: $P_{(r=0)} = 0$ and $P_{(r \geq Dmax)} = 0$, where D_{max} is the maximum particle extension. Due to the presence of larger particle species in solution, the p(r) function could only be determined for the mid-q-range $0.02/0.03 < q < 0.25$ $Å^{-1}$ for SAXS corresponding to the smaller particle species. From the corresponding pair distribution functions of the polyplexes the R_g values can be determined. To study

(6)

Radius of gyration defined by P(r)

$$R_g^2 = \frac{\int_0^{D_{max}} P(r)r^2dr}{2\int_0^{D_{max}} P(r)dr} \tag{7}$$

In SANS measurements, different contrasts were studied by varying H_2O to D_2O composition. The scattering length density and D_2O matching point was obtained by plotting I_0 against the D_2O concentration. The D_2O matching points for single mRNA and DEAE-Dextran solutions, as well as for the polyplexes were observed. The exact composition of the measured particles was determined. The remaining amount of water inside the particles was obtained by comparing the transmission of the particles with the transmission of the blank. The transmission of a sample is the ratio of the flux through the sample and the incident flux and can be a quantitative measurement of the hydrogen content of the sample or buffer. The log of transmission (normalized to sample thickness) is in linearity with the D_2O content of the buffer [45]. Guinier plots [46] of the scattering profiles according to eq. (8) were done to obtain the radius of gyration R_g.

Logarithmic Guinier equation

$$\ln(I(q)) = \ln(I_0) - \frac{R_g^2}{3}q^2 \tag{8}$$

3. Results

3.1. Potentiometric titration

The N/P ratio is defined as the ratio of moles of the amine (N) groups of cationic polymers to those of the phosphate (P) groups of mRNA/DNA [47]. An N/P ratio of 1 is equal to the same amount of phosphates and amines in the system, irrespective of its charge. DEAE-Dextran is a modified natural polymer consisting of three different monomers (Fig. 1a). In general, 2-Chloro-N,N-dimethylethylamine hydrochloride is coupled with purified Dextran to form DEAE-Dextran. This reaction results in two tertiary amines with different pK_a as well as a permanently positively charged quaternary amine. The percentage content of the respective amines can be determined by means of potentiometric titration. Therefore, the coefficient between the change in pH and the change in volume (ΔpH/ΔV) against the added volume of titrant is observed (Fig. 1b). The two tertiary amines are positively charged in a pH-dependent manner. Deflections occur each time an amine is completely unionized. By means of the exact weighing, the volume and the molarity of added titrant, it can be determined that 0.99% of the total mass can be referred to the nitrogen of the weaker tertiary amine and 0.74% of the total mass can be referred to the nitrogen of the stronger tertiary amine. The amount of the quaternized amine is equal to the amount of the weaker tertiary amine (Fig. 1a). This results in a total mass of 2.72% amine for the processed DEAE-Dextran in dry mass. Further calculation leads to a distribution of the three monomers to be A:B:C = 6:1:1. To keep the amount of ionized amines constant, a constant pH of 7.2 was adjusted. Under these conditions, approx. 48% of tertiary amines and 100% of quaternary amines are ionized, resulting in 66.8% ionized amines. According to weight, a ratio of 1.125:1(w/w) DEAE-Dextran:mRNA would be necessary for an N/P ratio of 1. However, electrostatic interaction is pH sensitive. Therefore, an N/P ratio of 1 does not consequently result in a balanced net charge. Instead, pH dependent variations occur. The ionization of mRNA at pH 7.2 is 90%. Considering the ionization at a pH of 7.2, a

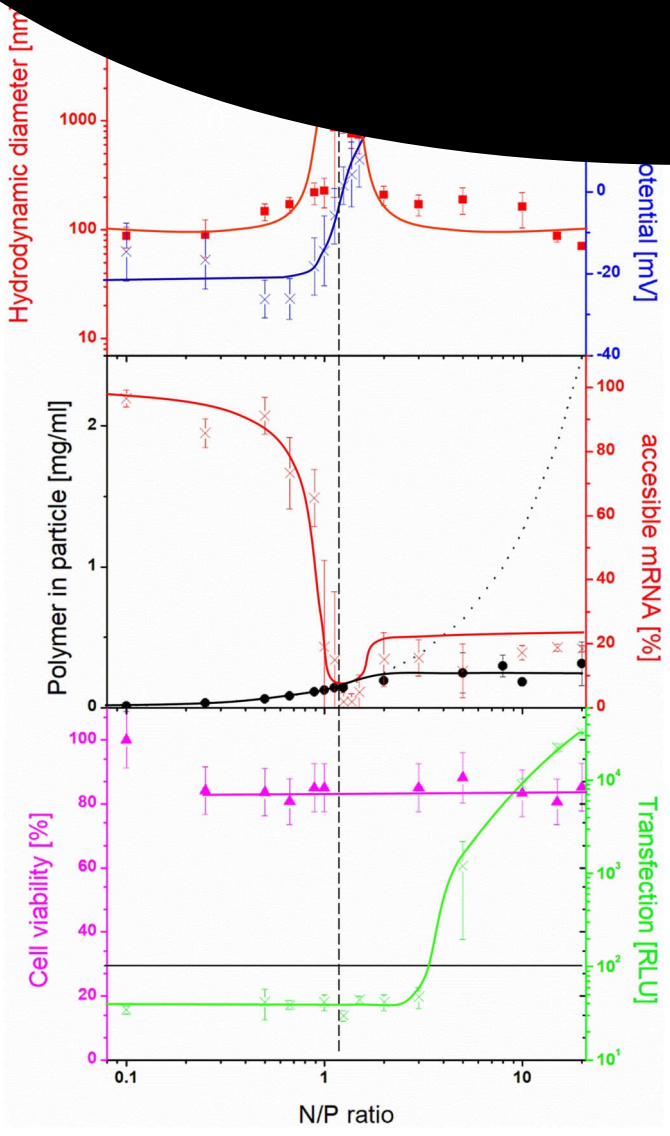

Fig. 2. Characterization of DEAE-Dextran/mRNA polyplexes. Top: hydrodynamic diameter (red line) and zeta potential (blue line) changes with respect to N/P ratio of DEAE-Dextran/mRNA polyplexes. Particle aggregation is observable at the inflection point of the sigmoidal zeta potential behavior (vertical black dashed line). Middle: Concentration of DEAE-Dextran in the particle (black). The free DEAE-Dextran was measured and subtracted from the total amount of DEAE-Dextran (black dots). In red: free accessible mRNA as measured from the Quant-it Ribogreen assay according to N/P ratio. Bottom: Cell viability (pink) and transfection (green) of DEAE-Dextran/mRNA polyplexes with respect to N/P ratio. All lines are drawn to guide the eye and do not represent any type of model fit. (For interpretation of the references to colour in this figure legend, the reader is referred to the Web version of this article.)

calculated 1.35-fold molar amount of amines (N/P ratio of 1.35) is required to have balanced net charge. With regards to the molar weight of the single compounds, an N/P ratio of 1 is equal to ~27 mol DEAE-Dextran per mol mRNA.

3.2. Variation of charge ratio

3.2.1. ζ potential, polydispersity and particle size

Polyplex nanoparticles were assembled by mixing of DEAE-Dextran and mRNA in different ratios, where the mixing ratio was expressed in terms of N/P ratio as outlined above. The variation of N/P ratio resulted in different regimes of distinct particle characteristics (Fig. 2, top),

[redacted] the $Z_{average}$ [redacted] positive zeta potential was measured. In the intermediate range (N/P ratio 1–2), particle size diverged, and the correlation curves (see supplementary data) did not allow meaningful analysis using the cumulant algorithm. Hence, the plotted particle sizes between the N/P ratio of 1–2 are not quantitatively meaningful and are shown to indicate the trend towards particle aggregation within this range. In the same range the zeta potential switched from negative to positive. Therefore, this is considered the range of charge equilibrium between positive and negative charges, where the net surface charge of the particles is not high enough for repulsion. Thus, particle aggregation occurs. Consequently, one may conclude that 1.1 to 1.5 nitrogen atoms in the polymer correspond to one positive charge, which is in alignment with the calculated N/P ratio of 1.35 to achieve a balanced net charge, as predicted from the potentiometric titration. With these overall characteristics, the polymer-based nanoparticles display in principal similar behavior as the previously described lipid based systems [6]. Here, the net charge of the polymer is not as well defined in comparison to that of a charged lipid, and it depends on solvent properties such as ionic strength and pH. Thus, the measurements as a function of molar ratio enabled to determine the actual mean charge per nitrogen atom in the polymer.

3.2.2. Measured Polymer amount in the particle/accessible mRNA

To further characterize the systems, both, polymer and mRNA concentration as a function of the N/P ratio were determined. As described in the methods section, an mRNA binding fluorescence dye was used in order to differentiate between accessible and non-accessible mRNA. In general, the amount of accessible mRNA decreased with an increase of DEAE-Dextran, and thus the N/P ratio. In the range of an N/P ratio of 1–1.5, no free mRNA is measurable. Due to the large particle size measured in DLS, and the visible aggregates in this range, it is suspected, that the mRNA is not present in the solution but bound to aggregate clusters. Interestingly, with an excess of polymer, above an N/P ratio of 2, 15–20% of the total mRNA was measured as accessible fraction. On the other hand, free DEAE-Dextran (Fig. 2, middle, black) can be subtracted from the provided amount to gain the actual DEAE-Dextran amount in the particle and therefore the actual N/P ratio. As the added amount of DEAE-Dextran is steadily increasing (dotted line), the amount of DEAE-Dextran in the particle remains constant between 45 and 58 mol DEAE-Dextran per mol mRNA. Therefore, the actual N/P ratio in the particle ceases between 1.7 and 2 ± 1, indicating a saturation of the polymer concentration in the particle.

3.2.3. RNA encapsulation efficiency and heparin release assay

To get further insight into structural and functional coherencies of the DEAE-Dextran nanoparticles, a model for charge-stimulated release was set up. Charge driven interactions with the endosomal membrane are considered to play a role for endosomal release of the mRNA cargo after cellular uptake. Gel electrophoresis of untreated and heparin treated particles was done as described above (Fig. 3). Non-heparin treated particles show undetectable mRNA irrespective of N/P ratio. Heparin is a naturally occurring glycosaminoglycan. It is negatively charged and has a high affinity for DEAE-Dextran. When sufficient amounts of heparin are added to the polyplex suspension, mRNA can be released from the polyplexes. For each particle, the same heparin:mRNA ratio was added. Released mRNA was detected for polyplexes within all observed N/P ratios. Comparing the intensities of released mRNA before and after heparin treatment, different intensities are visible. Stronger contrast bands can be observed for particles with higher N/P ratio. Hence, surprisingly, mRNA release is facilitated in particles with higher N/P ratios. This facilitated release could play a

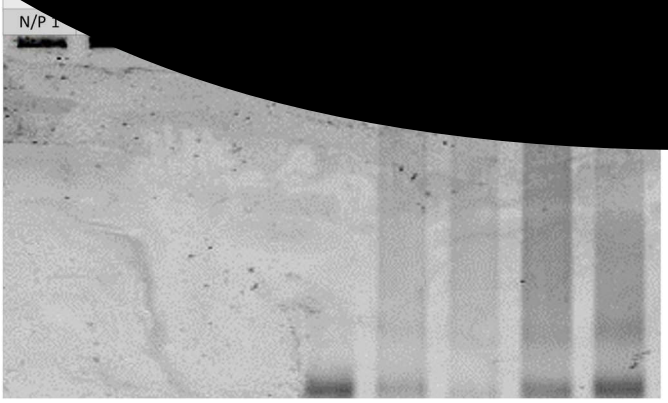

Fig. 3. Gel electrophoresis of DEAE-Dextran/mRNA polyplexes before (left) and after (right) Heparin release assay. mRNA bands are visible in different intensities after release. Positive control (mRNA) is the same mRNA in the same concentration as in the particles.

role for the observed higher transfection efficacy of such polyplexes and could as well be explained with a less pronounced binding site between DEAE-Dextran and mRNA.

3.2.4. Transfection of dendritic cells with DEAE-Dextran-mRNA polyplexes

Transfection of particles with different N/P ratios was measured and compared (Fig. 2, bottom). The cell viability after addition of DEAE-Dextran/mRNA particles is above 80% regardless of the N/P ratio, indicating no toxic effects of DEAE-Dextran irrespective of the added amount.

No cell transfection was measured for particles with negative charge excess. Biological activity could be measured with particles with an N/P ratio of 3 and higher. Within the range of an N/P ratio of 3–10, a strong increase is observed. Particles at an N/P ratio of 10 have a 10-fold higher uptake as particles at an N/P ratio of 5. As mentioned above, the DEAE-Dextran concentration in the particle is not increasing. However, the free DEAE-Dextran in higher N/P ratios have an adjuvant effect on the transfection efficiency. Another explanation for an increased transfection, however, might be a less pronounced binding between the DEAE-Dextran polymer and mRNA with increased amount of DEAE-Dextran. Due to an excess of DEAE-Dextran, more polymer chains are electrostatically attached to the mRNA and therefore, the binding span between DEAE-Dextran and mRNA is decreased. The variety of N/P ratio plays a large role in terms of transfection. Pharmaceutical relevant particles have an N/P ratio of 3.5–10. In this aspect, the DEAE Dextran particles display clearly different transfection characteristics than those formed from cationic lipids, which showed transfection both with positive and with negative charge excess. Further measurements will be necessary to elucidate the foundation of the poor transfection of the negatively charged polyplexes. For other polymer based systems (e.g. from polyethylenimine) it has been hypothesized, that excess of free polymer is required for good transfection efficacy. From the *in vitro* transfection, this hypothesis is supported but it needs to be clarified *in vivo* in future experiments.

3.2.5.

Small angle x-ray scattering (SAXS) measurements were performed with particles of an N/P ratio of 0 (free mRNA), 2 and 10. The amount of mRNA was kept constant at 0.1 mg/ml. The amount of DEAE-Dextran was calculated in mmol % positive charge with respect to the mmol amount negative charge of mRNA. For the calculations, 340.5 g/mol was taken as a basis for one mRNA repeat unit. This is equal to 2.94 mmol negative charge per g mRNA. The positive charge density of DEAE-Dextran was calculated with the help of potentiometric titration. The amount of positive charges is 1.94 mmol per g DEAE-Dextran. This

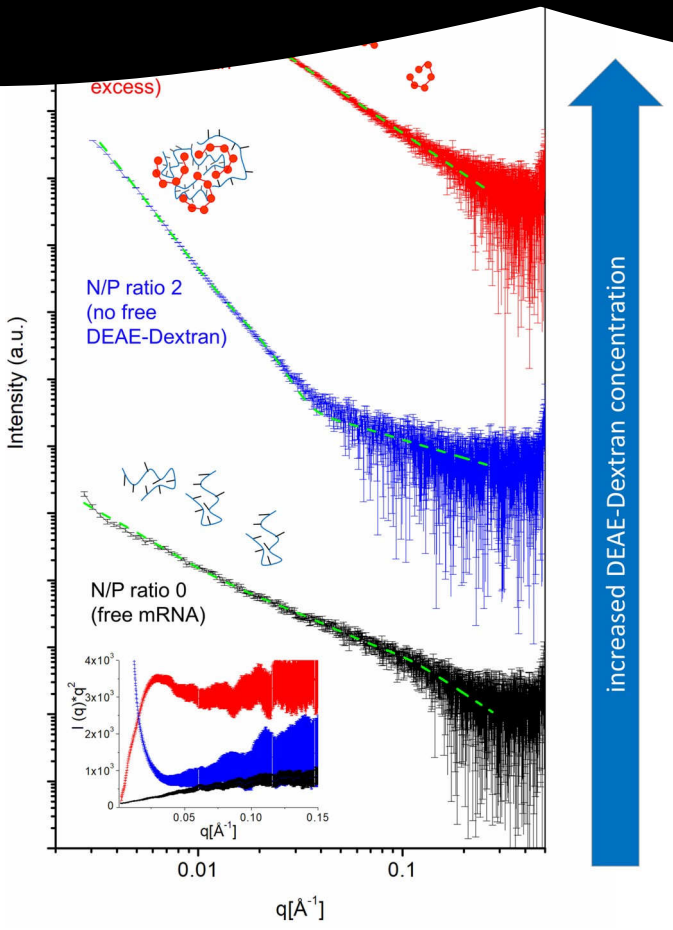

Fig. 4. SAXS data of DEAE-Dextran/mRNA polyplexes with an N/P ratio of 0 (black), 2 (blue) and 10 (red) in HBGx1 buffer (pH 7.2). Green dashed curves are fit models of the respective scattering curves obtained with *SASfit* using the unified exponential power law from *Beaucage* [38,39]. Data are shifted vertically for clarity. Kratky plot (bottom left inset plot) was obtained by plotting $I(q)*q^2$ against q. (For interpretation of the references to colour in this figure legend, the reader is referred to the Web version of this article.)

results in 0.31 mg/ml (N/P ratio 2) and 1.55 mg/ml (N/P ratio 10) DEAE-Dextran. Therefore, a 5-fold amount of DEAE-Dextran is present in the system at an N/P ratio of 10 compared to an N/P ratio of 2. According to the physicochemical analysis, polyplexes with an N/P ratio of 2 are considered the closest possible stable particles to the charge equilibrium, whereas particles with an N/P ratio of 10 displayed higher activity in the cell culture model.

Fig. 4 shows the scattering curves of free mRNA and polyplexes with two different N/P ratios. As expected for such type of particles, all scattering curves are unstructured, free of indication for ordered or repetitive arrays (no Bragg peaks). In that sense, the polyplex particles structurally differ from similarly assembled lipoplex particles obtained from liposomes and RNA [5,29]. Uncorrelated scattering from either individual molecules (mRNA) or polyplex nanoparticles can be taken into account for data analysis. Already by the eye, clearly, the differences between the curves for the free mRNA and the polyplexes at an N/P ratio of 2 can be outlined. The profile of the scattering curve at an N/P ratio 2 is approximately comparable to the profile of relatable polyplexes in literature [48]. With a further increase in DEAE-Dextran, the profile of the scattering curve changes again significantly. This can be due either to a change of the particulate organization going from, N/

tribution

Kratky plot
particle architecture
coil organization. As can be seen
in the corresponding Kratky plot (red curve), the
appears to comprise particles with partial globular character. In contrast, for an N/P ratio of 2, no clear indication for globular particles can be derived, which indicates, that particle characteristics may still change with increasing polymer excess. For free mRNA the structure is of even weaker globular character (presence of a weak shoulder in the Kratky plot).

In order to determine structural parameters from these curves systematically, the unified fitting model of *Beaucage* was used to analyse the SAXS data [38,39]. This approach allows describing complex systems containing multiple structural levels, as is the case for the given systems. The corresponding parameters are given in table S1 (supplementary data). The fit models of the respective curves are depicted as green dashed lines in Fig. 4. In order to get best representation of the data by the model curves, a fraction of particles with $R_{g1} \geq 100$ nm had to be taken into account. As the actual R_{g1} is beyond the resolution of the instrument this is not considered physically meaningful, and these values are not taken into account for the interpretation of the particle characteristics. Due to the presence of multistructural levels in the scattering curve, identities of smaller substructures could be derived by the pair distance distribution in the mid q-range for an N/P ratio of 0 and 10.

For an N/P ratio of 2, the SAXS curves exhibits a much steeper decay at small q-values, as well as a stronger forward scattering than for the N/P ratio of 10. The Guinier plots at $q < 0.02$ (data not shown) appear not to be linear over a reasonable q^2 regime, thus no radius of gyration was obtained at low q-values ($q < 0.02$). However, these findings are in accordance with the particle size analysis by DLS (Fig. 2), showing a diverged particle size for particles with an N/P ratio between 1 and 2 (Fig. S3). For the particles with an N/P ratio of 10, again no linear behavior was found in the Guinier plots at $q < 0.02$. Therefore, an apparent $R_g > 50$ nm is assumed. However, the forward scattering is less pronounced as in the SAXS curve of particles with an N/P ratio of 2.

Pair distance distribution functions of the scattering curves in the mid q-range ($0.02 < q < 0.3$), could be performed for an N/P ratio 0 (data not shown) and N/P ratio 10 (Fig. 5). For an N/P ratio of 0, D_{max} is ~13 nm and R_g is ~4 nm, which can be assigned to the free mRNA.

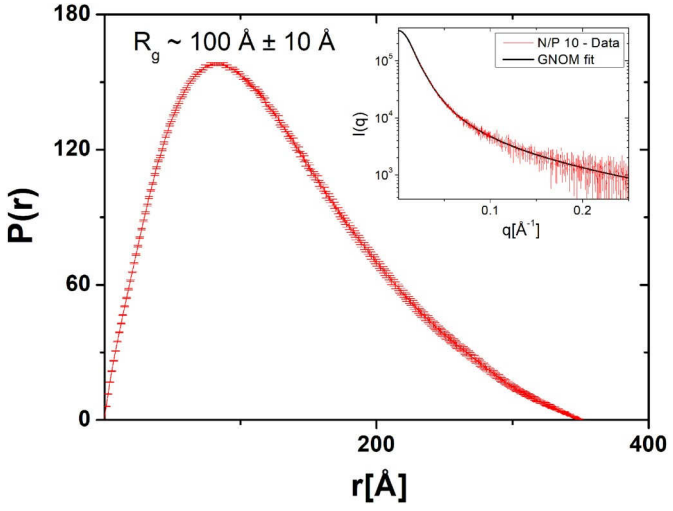

Fig. 5. Pair distance distribution function of the scattering curve at the N/P ratio 10, determined for the mid-q-range $0.03 < q < 0.3$ Å^{-1}. The Inset plot shows the experimentally obtained scattering curve and the GNOM fit extrapolated for all I(q).

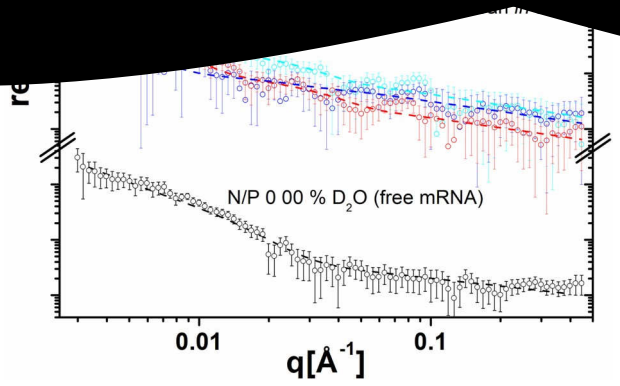

Fig. 6. SANS data of DEAE-Dextran-mRNA polyplexes (1.6 mg/ml) in HBGx1 buffer (pH 7.2). Plot shows measured scattering curves of particles at an N/P ratio of 8 at different H_2O/D_2O mixing ratios, as well as pure mRNA at 0% D_2O concentration (black curve). Dashed curves are fit models of the respective scattering curves obtained with *SASfit* using the unified exponential power law from *Beaucage*. Data are shifted vertically for clarity.

For an N/P ratio of 10, a subpopulation with a size of $D_{max} \approx 35$ nm and $R_g \approx 10$ nm was measured. This subpopulation is not detectable for an N/P ratio of 0 and 2. Therefore, this is associated to the system only when excess of DEAE-Dextran is present, such as the case at an N/P ratio of 10. The patterns may derive from free DEAE-Dextran, but also it cannot be excluded, that they derive from structures inside the polyplex particles or the second mRNA-containing fraction which was determined at high N/P.

3.2.6.

Fig. 6 shows several SANS scattering profiles, plotted against the scattering vector q. The scattering curves depict the same polyplex particles with the same N/P ratio but in different D_2O concentrations, as well as the scattering curve for free mRNA in H_2O buffer. Here, particles with an N/P ratio 8 were measured, which are considered similar to those measured in SAXS (exact N/P could not be matched due to technical reasons), where the amount of free DEAE-Dextran is 20–25% less. As well, SAXS was measured in only 10 mM HEPES and SANS was measured in the modified HBSS buffer, where the ionic strength was higher (~150 mM NaCl). The scattering curve of the free mRNA resembles the respective SAXS scattering curve. The obtained radius of gyration from the Guinier plot (Fig. S6) is approximately ~13 nm which is larger than the value form the comparable sample in SAXS measurements (~4 nm). This is considered to be due to differences in the composition of the buffer and the presence of aggregates which could not be completely avoided due to the restrictions for sample preparation at the SANS facility. Due to the lower count rate and the incoherent scattering background, no statement can be given for higher q values ($q > 0.2$).

Also, the SANS curved were modelled using the *Beaucage* formalism, however, for these data sets, it was not used to derive quantitative numbers due to higher statistical errors of the data. Therefore, the corresponding parameters are not discussed in detail but given in Table S1 (supplementary data).

Qualitatively, a change in the profile of the scattering curves between free mRNA (black dots) and mRNA in the particle (blue dots) can be seen. Therefore, a conformational change of mRNA can be expected between the free mRNA and the mRNA measured in the polyplexes at the matching point of DEAE-Dextran (33% D_2O). The scattering curves of matched DEAE-Dextran (blue) and matched mRNA (red), were very similar, which is in line with the assumption, that for both contrasts, the scattering resulted from the polyplex particles (and not free DEAE-

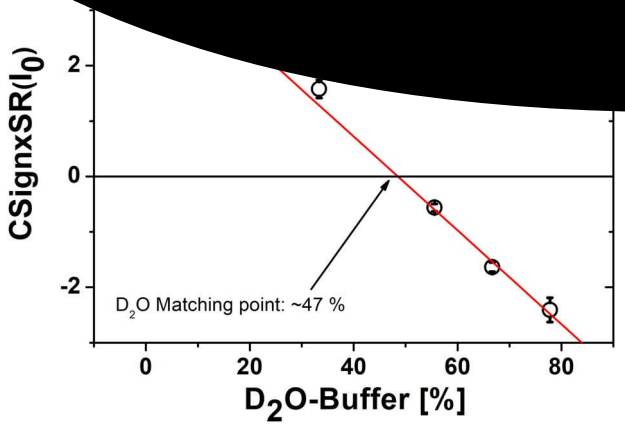

Fig. 7. Contrast matching point analysis. I_0 was obtained by extrapolating the scattering curve at low q values. The square root of I_0 plotted against the D_2O concentration in buffer yield the D_2O matching point and scattering length densities of DEAE-Dextran/mRNA polyplexes. The D_2O matching point is 47 ± 3%.

Dexran or RNA), where the internal distribution of both moieties was homogenous. Substructures could not be unequivocally revealed from the data, because of the too high statistical errors. Therefore, qualitative differences of the radial distribution must be investigated in further experiments.

The contrast matching point of DEAE-Dextran – mRNA polyplexes is 47 ± 3%. It was obtained by the x-intercept of a plot of $\sqrt{(I_0)}$ versus % D_2O (Fig. 7). Likewise, the contrast matching points of mRNA and DEAE-Dextran were obtained (Fig. S5). For mRNA, the D_2O matching point is ~65% and for DEAE-Dextran ~34%. Assuming that the scattering density of the material does not change upon binding to mRNA or DEAE-Dextran, the scattering curve for the complex in the respective buffer provides information about size and shape of the polyplex agents alone. Therefore, DEAE-Dextran is nearly completely matched at a D_2O concentration of ~33%, thus the obtained scattering curve is dedicated only to the scattering of mRNA *in situ*. Similarly, at ~66% D_2O mRNA is matched. Comparing the matching points of the single components (65% for mRNA and 34% for DEAE-Dextran) and the polyplex (47%), the actual mass ratio can be indicated for particles with an N/P ratio of 8. Fitting the polymer concentration to the scattering density reveals an mRNA content of ~42% by mass and an actual N/P ratio of the measured particle structure of ~1 ± 0.3. This in accordance with the previously made observation, that additional DEAE-Dextran (N/P ratio ≥ 2) is not incorporated into the particles.

4. Discussion

We have performed a systematic investigation of polyplex nanoparticle formation from DEAE-Dextran and mRNA, where the molar ratio between the two components was varied in a wide range. Using a set of independent scattering techniques (DLS, SAXS, SANS) in combination with further assays (binding studies, release characteristics and evaluation of biological activity) characteristic structural and functional parameters as a function of the manufacturing scheme were derived. The total amount of nitrogen in the DEAE-Dextran and the degree of ionization at physiological pH values were investigated by potentiometric titration of the individual substances. The molar ratio of DEAE-Dextran:mRNA to obtain the same amount of nitrogen and phosphate in the system (N/P ratio 1) was found to be approximately 27:1 and at a pH of 7.2 a calculated 1.35-fold molar amount of amines (N/P ratio of 1.35) was required to yield balanced net charge. This is in accordance with the results from the ζ potential, showing charge

[illegible] a constant [illegible]
[illegible] increased N/P ratio (N/P ratio > 2)
[illegible] 2, middle). Although this method is not as accurate as the contrast matching point analysis from SANS, it is in accordance with the other results, that the actual N/P ratio is slightly above or at the charge equilibrium.

Particles with the N/P ratio from 3 to 10 showed biological activity in the cell culture model applied here. Within this range, a positive ζ potential, narrow particle sizes, high encapsulation efficiencies, and increasing transfection rates were observed.

Although the excess of polymer increased, release of mRNA as determined by the heparin assay, was facilitated with increasing N/P ratio, indicating less affine binding sites of DEAE-Dextran to the mRNA at higher N/P ratios. As well gel electrophoresis indicated that a certain amount of accessible mRNA which is not completely free, but attached to DEAE-Dextran with increasing N/P ratio, was present. In that range, SAXS measurements indicated the presence of substructures in the length scale of 10–20 nm.

Taking all these findings together, a molecular model can be suggested where, in the excess of dextran, the system is more complex than consisting of just dextran/RNA nanoparticles and free polymer. These observations appear to be directly correlated with the biological activity, which increased with increasing polymer excess. Further investigation will be necessary to fully elucidate these coherencies. Such insight can be helpful for tailored development of improved mRNA delivery systems in the future.

5. Conclusions

Using DEAE-Dextran as a model polymer, parameters to form defined mRNA polyplex particles as delivery vehicles in a defined and reproducible manner were derived. By variation of the molar ratio between the two components, suitable regimes for particle formation were identified, which correlated to an excess of either negative or positive charge. By extended characterization, including of SAXS and SANS measurements, the mRNA delivery vehicles were analysed in order to improve understanding of the molecular organization inside these systems and to investigate their coherencies with the biological activity of the product. This demonstrates, that such advanced characterization can help to better understand product characteristics and find clues for defining product keys and product qualifications.

Author contributions

The manuscript was written through contributions of all authors. All authors have given approval to the final version of the manuscript. Further, the authors would like to acknowledge the contribution of Cristina Sala for the graphical abstract.

Conflicts of interest

The authors report no competing financial interest.

Acknowledgements

The authors gratefully acknowledge funding by Max Planck Graduate Center (MPGC-Mainz), the BMBF (FKZ: 131A026C) and the “Deutsche Forschungsgemeinschaft” (SFB 1066). We thank Jozef Al-Gousous, Mark Denny, Michael Hofmann, Michael Klak and Lukas Uebbing for their advice and support. The graphical abstract has been contributed by Cristina Sala.

Supplemen

doi.org/10.1016/j.bio

References

[1] U. Sahin, K. Karikó, Ö. Türeci, "mRNA-based therapeutics — developing a new class of drugs, Nat. Publ. Gr. 13 (2014).
[2] C.M. Koebel, et al., Adaptive immunity maintains occult cancer in an equilibrium state, Nature 450 (7171) (Dec. 2007) 903–907.
[3] S. Kreiter, et al., Mutant MHC class II epitopes drive therapeutic immune responses to cancer, Nature 520 (7549) (2015) 692–696.
[4] S. Pascolo, Vaccination with messenger RNA (mRNA), Handb. Exp. Pharmacol. (183) (2008) 221–235.
[5] S. Grabbe, H. Haas, M. Diken, L.M. Kranz, P. Langguth, U. Sahin, Translating nanoparticulate-personalized cancer vaccines into clinical applications: case study with RNA-lipoplexes for the treatment of melanoma, Nanomedicine 11 (20) (Oct. 2016) 2723–2734.
[6] L.M. Kranz, et al., Systemic RNA delivery to dendritic cells exploits antiviral defence for cancer immunotherapy, Nature (2016) 1–16.
[7] E. Grudzien-Nogalska, et al., Synthetic mRNAs with superior translation and stability properties, Methods Mol. Biol. 969 (2013) 55–72.
[8] Y. Wang, et al., Systemic delivery of modified mRNA encoding herpes simplex virus 1 thymidine kinase for targeted cancer gene therapy, Mol. Ther. 21 (2) (Feb. 2013) 358–367.
[9] G. Tavernier, O. Andries, J. Demeester, N.N. Sanders, S.C. De Smedt, J. Rejman, mRNA as gene therapeutic: how to control protein expression, J. Control. Release 150 (3) (Mar. 2011) 238–247.
[10] M.A. Dobrovolskaia, M. Shurin, A.A. Shvedova, Current understanding of interactions between nanoparticles and the immune system, Toxicol. Appl. Pharmacol. 299 (2016) 78–89.
[11] T. Merdan, J. Kopecek, T. Kissel, Prospects for cationic polymers in gene and oligonucleotide therapy against cancer, Adv. Drug Deliv. Rev. 54 (2002) 715–758.
[12] Y.-W. Yang, J.-C. Yang, Studies of DEAE-dextran-mediated gene transfer, Biotechnol. Appl. Biochem. 25 (1) (Feb. 1997) 47–51.
[13] A. Vaheri, J.S. Pagano, Infectious poliovirus RNA: a sensitive method of assay, Virology 27 (3) (Nov. 1965) 434–436.
[14] V.A. Maes R, W. Sedwick, Interaction between DEAE-dextran and Nucleic Acids vol. 134, (1966) no. 1967.
[15] K.D. Mack, R. Wei, A. Elbagarri, N. Abbey, M.S. McGrath, A novel method for DEAE-dextran mediated transfection of adherent primary cultured human macrophages, J. Immunol. Methods 211 (1–2) (1998) 79–86.
[16] D. Le Cerf, A.S. Pepin, P.M. Niang, M. Cristea, C. Karakasyan-Dia, L. Picton, Formation of polyelectrolyte complexes with diethylaminoethyl dextran: charge ratio and molar mass effect, Carbohydr. Polym. 113 (2014) 217–224.
[17] S. Pustylnikov, D. Sagar, P. Jain, Z.K. Khan, Targeting the C-type lectins-mediated host-pathogen interactions with dextran, J. Pharm. Pharm. Sci. 17 (3) (2014) 371–392.
[18] Y. Qian, et al., Targeting dendritic cells in lymph node with an antigen peptide-based nanovaccine for cancer immunotherapy, Biomaterials 98 (2016) 171–183.
[19] F. Nguyen, J. Szoka, Nucleic acid delivery : the missing pieces of the puzzle ? Acc. Chem. Res. 45 (7) (2013) 1153–1162.
[20] P. Menon, T.Y. Yin, M. Misran, Preparation and characterization of liposomes coated with DEAE-Dextran, Colloids Surfaces A Physicochem. Eng. Asp. 481 (2015) 345–350.
[21] S. Qian, R. Dean, V.S. Urban, B.N. Chaudhuri, The internal organization of mycobacterial partition assembly: does the DNA wrap a protein core? PloS One 7 (12) (2012).
[22] V.D. Badwaik, E. Aicart, Y.A. Mondjinou, M.A. Johnson, V.D. Bowman, D.H. Thompson, Structure-property relationship for in vitro siRNA delivery performance of cationic 2-hydroxypropyl-β-cyclodextrin: PEG-PPG-PEG polyrotaxane vectors, Biomaterials 84 (2016) 86–98.
[23] S.-F. Peng, et al., Effects of the nanostructure of dendrimer/DNA complexes on their endocytosis and gene expression, Biomaterials 31 (2010) 5660–5670.
[27] H.B. Stuhrmann, Small-angle scattering and its interplay with crystallography, contrast variation in SAXS and SANS, Acta Crystallogr. Sect. A Found. Crystallogr. 64 (1) (Jan. 2008) 181–191.
[28] International Conference on Harmonisation, Pharmaceutical development Q8, Guidel. Pharm. Dev. Q8 (August) (2009) 1–28.
[29] A. Ziller, et al., Incorporation of mRNA in lamellar lipid matrices for parenteral administration, Mol. Pharm. 15 (2018) 642–651.
[30] A.N. Kuhn, et al., Phosphorothioate cap analogs increase stability and translational efficiency of RNA vaccines in immature dendritic cells and induce superior immune responses in vivo, Gene Ther. 17 (8) (2010) 961–971.
[31] F.U. Gast, P.J. Hagerman, Electrophoretic and hydrodynamic properties of duplex ribonucleic acid molecules transcribed in vitro: evidence that A-tracts do not generate curvature in RNA, Biochemistry 30 (17) (Apr. 1991) 4268–4277.
[32] P. Kebbekus, D.E. Draper, P. Hagerman, Persistence length of RNA, Biochemistry 34 (13) (Apr. 1995) 4354–4357.
[33] J.A. Abels, F. Moreno-Herrero, T. van der Heijden, C. Dekker, N.H. Dekker, Single-molecule measurements of the persistence length of double-stranded RNA, Biophys. J. 88 (4) (Apr. 2005) 2737–2744.
[34] P. Khoshakhlagh, et al., Fasted-State simulated intestinal fluid "FaSSIF-C", a cholesterol containing intestinal model medium for in vitro drug delivery development, J. Pharm. Sci. 104 (7) (Jul. 2015) 2213–2224.
[35] S.M. Graetz L, Handbuch der Electrizität und des Magnetismus vol. II., (1921) [Online]. Available: https://archive.org/stream/handbuchderelek01graegoog/handbuchderelek01graegoog_djvu.txt , Accessed date: 6 April 2018.
[36] C.E. Blanchet, et al., Versatile sample environments and automation for biological solution X-ray scattering experiments at the P12 beamline (PETRA III, DESY), J. Appl. Crystallogr. 48 (2) (Apr. 2015) 431–443.
[37] A. Round, et al., BioSAXS Sample Changer: a robotic sample changer for rapid and reliable high-throughput X-ray solution scattering experiments, Acta Crystallogr. Sect. D Biol. Crystallogr. 71 (1) (Jan. 2015) 67–75.
[38] G. Beaucage, Small-angle scattering from polymeric mass fractals of arbitrary mass-fractal dimension, 29 (1996) 134–146.
[39] G. Beaucage, Small-angle scattering, J. Appl. Cryst. 28 (1995) 717–728.
[40] I. Breßler, J. Kohlbrecher, A.F. Thünemann, SASfit: a tool for small-angle scattering data analysis using a library of analytical expressions, J. Appl. Cryst. 48 (2015) 1587–1598.
[41] C.D. Putnam, M. Hammel, G.L. Hura, J.A. Tainer, X-ray Solution Scattering (SAXS) Combined with Crystallography and Computation: Defining Accurate Macromolecular Structures, Conformations and Assemblies in Solution, (2018).
[42] D.I. Svergun, Determination of the regularization parameter in indirect-transform methods using perceptual criteria, J. Appl. Crystallogr. 25 (4) (Aug. 1992) 495–503.
[43] C.E. Blanchet, D.I. Svergun, Small-angle X-ray scattering on biological macromolecules and nanocomposites in solution, Annu. Rev. Phys. Chem. 64 (2013) 37–54.
[44] D. Franke, et al., *ATSAS 2.8* : a comprehensive data analysis suite for small-angle scattering from macromolecular solutions, J. Appl. Crystallogr. 50 (4) (Aug. 2017) 1212–1225.
[45] D.I. Svergun, M.H.J. Koch, P.A. Timmins, R.P. May, Small Angle X-Ray and Neutron Scattering from Solutions of Biological Macromolecules, OXFORD University Press, 2013, pp. 75–77.
[46] A. Guinier, La diffraction des rayons X aux très petits angles : application à l'étude de phénomènes ultramicroscopiques, Ann. Phys. 11 (12) (Apr. 1939) 161–237.
[47] Q.-Q. Zhao, et al., N/P ratio significantly influences the transfection efficiency and cytotoxicity of a polyethylenimine/chitosan/DNA complex, Biol. Pharm. Bull. 32 (4) (2009) 706–710.
[48] I.C. Bellettini, S.J. Fayad, V.G. Machado, E. Minatti, Properties of polyplexes formed through interaction between hydrophobically-modified poly(ethylene imine)s and calf thymus DNA in aqueous solution, Soft Matter 13 (2017) 2609.